Evaluation of Ice-Coupled and Elevated GPR Antenna Acquisition on Ice

Tyler MacFarlane and Robert J. Ferguson

ABSTRACT

Two acquisition methods for near surface Ground Penetrating Radar (GPR) are compared for acquisition in ice-over-fresh-water-over-ground environments. In the first method, the antennae are coupled directly to the ice as in conventional acquisition. In the second approach, the antennae are elevated 0.5 m above the ice surface to mimic floatation of the antennae. Numerical comparison of reflectivity suggests that no significant degradation of signal results from elevation of the antennae relative to the ice-coupled. We verify the numerical result with a real-data acquisition at Ghost Lake, Alberta. Data acquired over the same linear traverse are compared, and no significant degradation of the target signal, ice-thickness and the lake bottom, is apparent.

INTRODUCTION

Ice has a very low dielectric permittivity which tends to cause strong reflections at interfaces with other materials (Finlay et al., 2008). So, waves that reflect from contacts such as an ice-water and water-ground boundaries are detectable by the GPR equipment. Ice also has a low electrical conductivity, and this property allows a great depth of penetration and a high signal to noise ratio (Jol, 2009).

Increased distance between GPR antennas and a target decreases subsequent GPR imaging (Sensors and Software, 2001). In glacial surveying, however, airborne GPR has been used for decades, where a low-frequency apparatus is flown a few hundred meters above the ice surface (Waite and Schmidt, 1961; Sen et al., 2003). Another common use of elevated radar antennas, which parallels the focus of this experiment, is surveying for defects in roads where antennas are slightly above the pavement (Saarenketo and Scullion, 2000).

Where radar is used in aircraft altimeters, it is known that ice has very similar electrical properties to air which makes it difficult to detect a boundary between the two (Waite and Schmidt, 1961). Since low frequency radar is not capable of resolving this contrast between ice and air, it appears transparent (Waite and Schmidt, 1961). Such a result suggests the following hypothesis: in glaciated regions, any negative impact on GPR that results from elevation above the surface of the antennas will partially offset due to the transparent nature of the air / ice interface. This hypothesis is supported by research performed in the Antarctic where airborne radar surveys are used to map sub ice structures beneath 3 km of ice (Sen et al., 2003). For such surveys, the system is flown approximately 300m above the ground and interpretable images are produced (Sen et al., 2003).

To avoid spatial aliasing, and so that very high-accuracy images can be obtained, GPR trace spacing must be sub-decimetre for most ground conditions (Grasmueck et al., 2005). Then, if unaliased data are to be acquired over a large area, for example a square kilome-

tre, datasets of approximately 10^8 traces would result. Such large acquisition requires a significant field effort.

With the exception of large 2D acquisition, as is practised in the Antarctic (Carter et al., 2009, for example), 3D acquisition is most often done by a crew of two or more people, and an apparatus comprising either connected antennae, or antennae - plus a recording system - that are attached to a sled or rolling frame, is used to couple the antennae directly to the ground or very close to the ground. In most cases where the antennae and recorder are on the ground (or close to the ground), acquisition requires constant human attention, and this exposes the human operators plus the recording system to environmental risks such as extreme weather and / or animals for long periods of time. Further, when the apparatus is in contact directly with the ground, or in contact through a wheeled or skidded chassis, rough terrain will induce significant, high-frequency variability between traces that will pose a significant challenge in data processing.

As a remedy for these problems, and in anticipation of achieving much higher acquisition rates, we posit a new apparatus for GPR as follows: Erect pylons at each corner of the acquisition grid. Suspend the antennae from wires anchored to each pylon with a motorized spooling system to enable positioning of the antennae within the acquisition grid. Computer control over the motor system would prevent interaction of the apparatus with the ground, and through wireless telemetry, the recording system and the operators could remain in a shelter. Acquisition time and effort would be reduced significantly, data security and human safety would be drastically improved, and trace-to-trace variability would be suppressed due to the smooth traverse of the suspended apparatus.

To justify construction of such an apparatus, it must be determined whether suspension of the radar results in significant signal degradation. Such degradation might be expected due to the added column of air between the apparatus and targets in the subsurface. Here, we choose a simple ice-over-water-over-ground scenario that is an analogue for glacial conditions. Specifically, we acquire data from the frozen lake surface of Ghost Lake Alberta due to it's close proximity to our research facilities. To anticipate success or failure for suspended radar, and to help guide acquisition design, we employ simple synthetic modelling to determine theoretical reflection coefficients and travel times.

Using a 4 medium model of the Earth (air-ice-water-soil), data quality is analyzed for both coupled and suspended acquisition methods to see if differences in resolution and interpreted properties arise. Direct measurements of layer thickness and literature values of ice-velocity provide controlled standards with which to compare the accuracy of interpreted GPR results.

THEORY

Ground penetrating Radar uses two antennas in transmitter/receiver pair to emit an EM wave into the subsurface and detect its reflections back to the surface (Daniels, 2004). By exploiting the fundamental physics of the wave propagation, reflected energy that is detected by the receiver can be interpreted in a non-destructive manner (Jol, 2009).

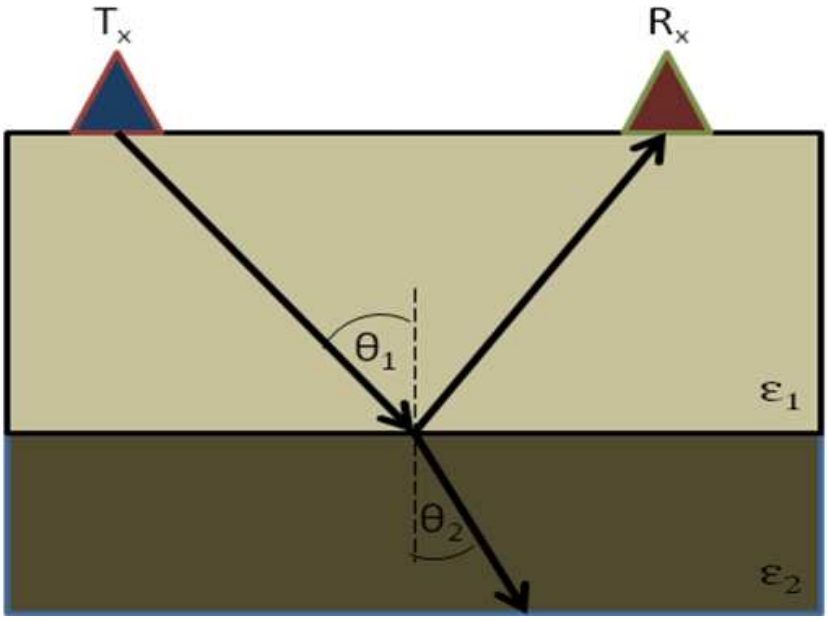

FIG. 1. Basic GPR ray paths that show reflected and transmitted waves.

Reflection and transmission

Three electric characteristics $(\varepsilon, \sigma, \text{and } \mu)$ control EM wave propagation in isotropic matter (Barger and Olsen, 1987, pg. 380). In terms of our interest in reflection and transmission of EM waves, dielectric permittivity (ε), a measure of a mediums ability to have its charge polarized by an electric field (Daniels, 2004), is the most important, as it largely controls reflection and transmission (Barger and Olsen, 1987, pg. 382). Electrical conductivity (σ) is characteristic of the ability of a material to conduct an electric current, and it is frequency dependent (Sato, 2001). Conductive materials diffuse EM waves rapidly, and this significantly restricts the range, and therefore the utility, of EM wave propagation (Jol, 2009). Fortunately, for air and ice, $\sigma \simeq 0$. Magnetic permeability (μ) is the extent of magnetization that a material obtains in response to a magnetic field (Jol, 2009). Like σ, μ is also frequency dependent.

In a dielectric (a weakly conductive material that is polarized by an electric field), $\sigma \sim 0$, and μ is approximately constant. The properties of a dielectric are approximately frequency independent, and only ε (dielectric permittivity) is significant. Here, for simplicity, we assume that air, ice, and ground are dielectric.

When the transmitting antenna of the GPR emits an EM wave, the wave propagates in all directions until it reaches an interface between materials determined by $\Delta\varepsilon$ - a change in dielectric permittivity (Barger and Olsen, 1987, pg. 382). This contrast causes a portion of the wave's energy to be reflected back to the surface while the rest is transmitted into the next layer (Figure 1). Snell's Law of refraction determines the geometry of the ray path shown in Figure 1 according to

$$n_1 \sin\theta_1 = n_2 \sin\theta_2 = p, \tag{1}$$

where, for the j^{th} layer

$$n_j \sim \sqrt{\frac{\varepsilon_j}{\varepsilon_0}}, \tag{2}$$

and $\varepsilon/\varepsilon_0$ is a measure of the reduction of an electric field in a dielectric (Barger and Olsen, 1987, pg. 160) relative to empty space. Angles θ_j and θ_{j+1} are the incident and transmitted angles respectively. Refractive index n_j is associated with the relative speed of a EM wave in the j^{th} medium.

Relative magnitudes of the reflected and transmitted rays are determined by Fresnel equations which are expressed as:

$$R = \frac{n_1 \cos\theta_1 - n_2 \cos\theta_2}{n_1 \cos\theta_1 + n_2 \cos\theta_2}, \tag{3}$$

and

$$T = \frac{2\, n_1 \cos\theta_1}{n_1 \cos\theta_1 + n_2 \cos\theta_2}, \tag{4}$$

where R is the reflection coefficient and T is the transmission coefficient (Barger and Olsen, 1987, pg. 392).

A common simplification in GPR studies is to assume normal incidence in calculations to find reflection depths and velocity information (Sato, 2001). In surveys where the targeted boundaries are shallow relative to the antenna spacing, an error in the predicted travel times and a reflection coefficient is introduced. Such is the case for data acquired in this experiment, antenna spacing was 1m, and the first reflector of interest is known to be only 0.55m deep. Through the application of trigonometry to the known geometry of the first 2 layers, the expected incident angles are calculated. For example, at the air-ice (elevated antennas) and ice-water (ice-coupled antennas) interfaces, the incident angles are 45^o and 42^o respectively. This is a significant deviation from the normal offset assumption. As the depth to the reflector increases, the ray paths more closely approximate normal incidence.

Modelling examples

A theoretic model of the impulse response at several boundaries shows how antenna elevation affects the measured data (Margrave, 2010). This model uses ray tracing based on Snell's law (1) to determine the incident and transmission angles at various boundaries for numerous rays. Each ray corresponds to a calculated antenna offset which the impulse response is plotted against. The expected impulse response represents the expected signal amplitude measured by the receiver and is calculated using equations 3 and 4. The impulse response accounts for transmission losses and the non-normal incidence of each refection. A cross-section of the assumed geometry is shown in Figure 2. Figure 3 shows the expected result of a degraded impulse responses when antennas are elevated. The most pronounced difference in amplitude for the two acquisition methods occurs at the ice-water boundary (green lines in Figure 3) while a smaller contrast is seen at the soil lake bottom (black lines in Figure 3). When the antennas are raised off the ground, a portion of the energy is reflected off the air-ice interface which reduces the amplitude of all reflections below (blue line in Figure 3). In ice-coupled data, this air-ice interface is not present and thus this additional energy loss does not occur.

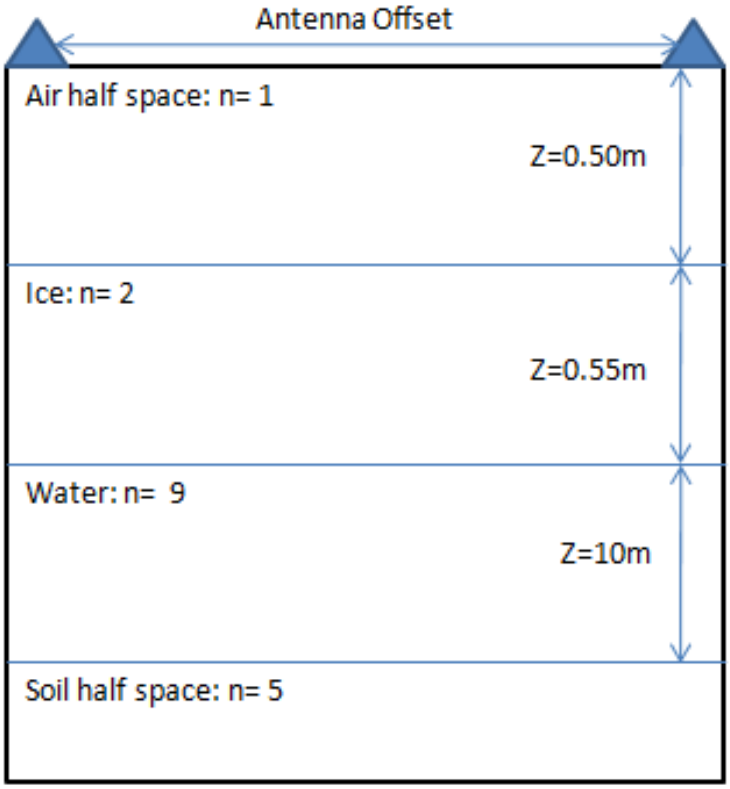

FIG. 2. Cross-section of layers used in the impulse response model. Z is the layer thickness and n is the refractive index.

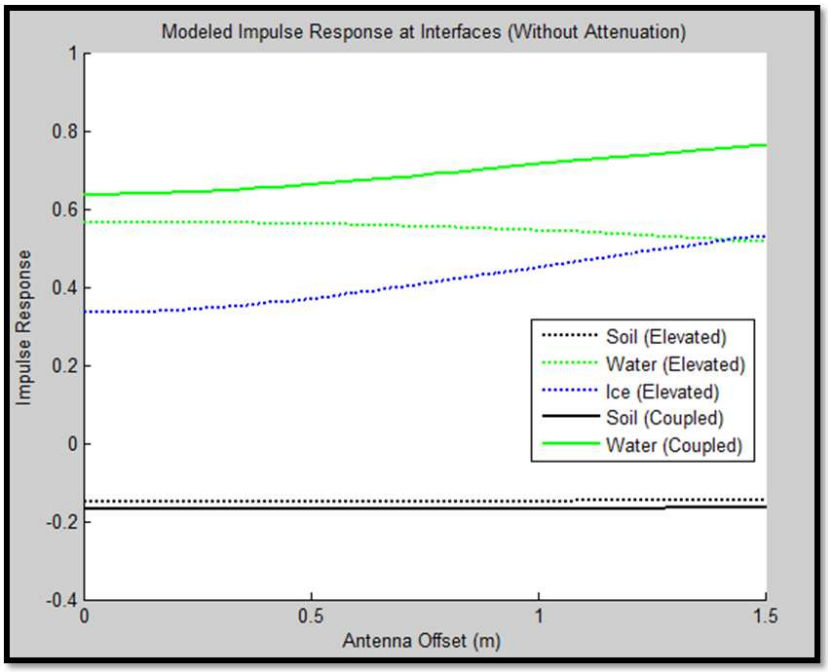

FIG. 3. Modelled impulse responses from known interfaces. Note that data modelled assuming elevated antennas are shown as dotted lines.

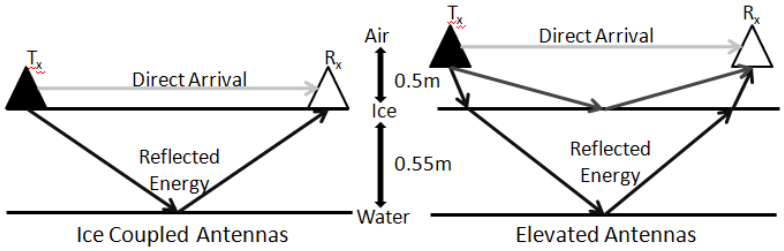

FIG. 4. Near surface ray paths (direct arrivals and reflections). A) Shows the case when the antennas are coupled with the ice. B) Shows the case when the antennas are elevated.

Travel-time analysis

Energy from direct arrivals and reflections at air-ice and ice-water boundaries have expected arrival times due to known ray path geometry (Figure 4) and velocity values found in literature (Daniels, 2004). Calculations of these expected travel times provide a reference to identify reflections in the data. Accurate values which factor in antenna offset will be determined along with values calculated assuming normal incidence.

Direct arrivals

Direct arrivals waves arrive to the receiver via a straight ray path from the transmitter (Fisher et al., 1992). It is defined by:

$$\Delta t_{DA} = \frac{\Delta x}{v_{air}} = 3ns, \tag{5}$$

where Δx is the antenna spacing (1m) and v is the velocity of light in air which equals 3×10^8. The direct arrival times for both elevated and ice-coupled data will be the same due to constant antenna offset.

Ice reflections

Travel times of energy reflected on the air-ice and ice-water interface are calculated based on ray path geometry determined by Snell's law (equation 1). The basic equation for calculating travel time (Δt) is:

$$\Delta t_{DA} = \frac{d}{v_{layer}}, \tag{6}$$

where d is the distance travelled by the ray path, and v_{layer} is the velocity of the wave in a specified layer.

Ice-water reflections (Ice-Coupled Antennas)

For the ice-water reflection in the ice coupled data, the distance travelled by the EM wave is

$$d = 2\sqrt{\left(\frac{\Delta x}{2}\right)^2 + z_{ice}^2}, \tag{7}$$

where Δx is the antenna offset, and $z_{ice} = 0.55$m is the ice thickness. The travel time is then expressed as:

$$\Delta t_{DA} = \frac{d}{v_{ice}} = 7.01ns, \tag{8}$$

where $v_{ice} = 2.12 \times 10^8$ m/s is the velocity of EM waves in ice. When Normal incidence is assumed, the distance travel by the wave is:

$$d = 2\, z_{ice} = 1.1\text{m}. \tag{9}$$

The travel time is calculated to be:

$$\Delta t_{\perp} = \frac{2 z_{ice}}{v_{ice}} = 5.20ns. \tag{10}$$

This is a difference in computed travel times of 1.81 ns which is a 26 % error in the events expected arrival.

Air-Ice Reflection (Elevated Antennas)

The first reflection in data acquired with suspended antennas is from the air-ice boundary. The distance ravelled by the ray path is given by:

$$d = 2\sqrt{\left(\frac{\Delta x}{2}\right)^2 + z_{air}^2} = 1.41\text{m}, \tag{11}$$

where $z_{air} = 0.5$ m is the height of antennas above the ground. Event travel time is given by:

$$\Delta t = \frac{d}{v_{air}} = 4.71ns, \tag{12}$$

where $vair = 3 \times 10^8$ m/s. When the assumption of zero offset is used, the calculated travel time becomes:

$$\Delta t_{\perp} = \frac{2 z_{air}}{v_{air}} = 3.33ns. \tag{13}$$

This amounts to a difference of 1.38 ns which is a 29 % error.

Air-water Reflection (Elevated Antennas)

Reflection for this event is more complicated due to the wave propagating in 2 different mediums. The Matlab code used to model the impulse response determines the ray path geometry as part of its workflow. The distance travelled by a ray which reflects off the ice water contact when the antennas are elevated is:

$$d = d_{air} + d_{ice} = 1.21\text{m} + 1.15\text{m} = 2.36\text{m}. \tag{14}$$

Since the ray spends time in 2 different velocity zones, the total travel time is the sum of the time it takes to traverse each medium. It is expressed as:

$$\Delta t = \frac{d_{air}}{v_{air}} + \frac{d_{ice}}{v_i ce} = 9.43\text{ns}. \tag{15}$$

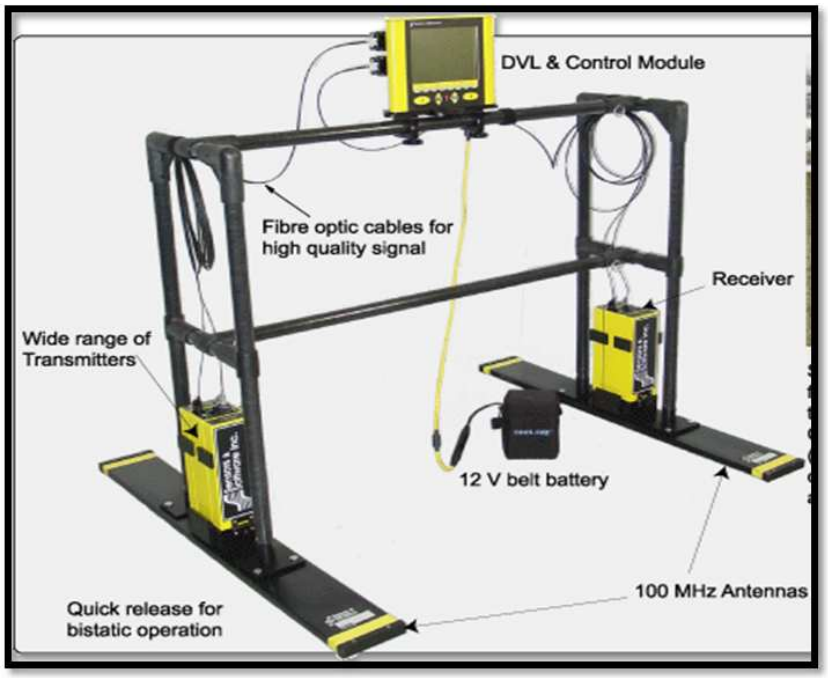

FIG. 5. The PulseEKKO PRO GPR system with all components labelled (from Sensors and Software (2001)).

Applying the normal incidence assumption determines a time value of:

$$\Delta t_{\perp} = \frac{2\,z_{air}}{v_{air}} + \frac{2\,z_{ice}}{v_{ice}} = 8.52\text{ns}. \tag{16}$$

The discrepancy between these two values is 0.91ns which is an error of 10%. For surveys where accurate calculations are necessary, ray paths should not be assumed to be normal incidence because large errors will be obtained. This is especially true when the reflectors are very shallow relative to the antenna spacing, which is shown by the above analysis. As the reflectors became deeper, the simplified and realistic travel time calculations become closer to each other. For the model used in this experiment, errors in expected travel times can be up to 29 % if this assumption is used.

SURVEY

Radar equipment

Equipment used for this project was provided by the University of Calgary Geoscience department and CREWES (Consortium for Research in Elastic Wave Exploration Seismology). The acquisition system is a Sensoft produced PulseEKKO PRO GPR (Figure 5). Components of a GPR system are include a receiver, transmitter, antennas, battery pack, control module, and fibre optic cable to connect the system. Data processing was performed with Sensoft's standard interpretation program called WIN EKKO PRO.

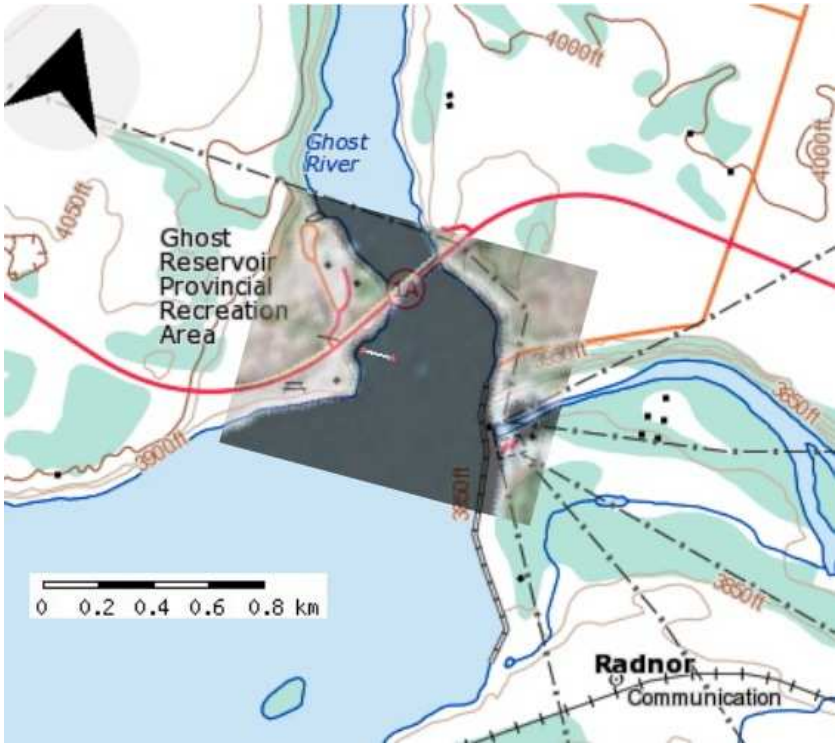

FIG. 6. Map location of the radar line on Ghost Lake (Adapted from Mitchell (1991)). The line is the short segment in white with red ends just SW of highway 1A.

Ghost Lake

Data was acquired from Ghost Lake, Alberta located 45 km west of Calgary along highway 1A. Figures 6 and 7 show the location of the site on a map that contains water depth contours. Due to high variability in lakes depth, the test site was chosen at a location with a shallow water depth and a small dip in the lake floor to give the highest probability of imaging the lake bottom.

Ghost Lake covers 11.0 km2 and was created from the completion of TransAlta Corporations dam in 1929 that is used to produce hydroelectric energy. The mean water depth is 15m, with various segments reaching up to 34m. This water is very fresh with it's electrical conductivity measured to be 277 ± 14.4 mS/m (Mitchell, 1991). Low conductivity is necessary for GPR surveys to attain a large depth of penetration (Barger and Olsen, 1987). At the time of data acquisition, the ice depth at the survey location was 0.55m. Data was acquired along a 100m survey line which started at an offshore buoy, and progressed due west towards the shore (Figure 8). Four rocks were wrapped in tinfoil and frozen 55 cm into the ice via augured holes at 20 m intervals along the line. Reflectors were implanted a week before the data was acquired to ensure the holes were completely frozen; thus reflections in the data would arise from dielectric contrasts caused by a rock-ice interface, and not a column of water in the ice. A strong dielectric contrast between the tinfoil and ice are expected to produce large reflections that can be used to calibrate the migration and function as reference points for quality control.

The dataset was broken into 4 segments that are labelled Line 00 to 03 (Figure 8). This

FIG. 7. Map location of the radar line on Ghost Lake (Adapted from Mitchell (1991)). The line is the short segment in white with red ends just SW of highway 1A.

study will focus on the data in lines 01 and 02 because they provided a direct comparison of ice coupled and suspended antenna acquisition systems. Line 01 contains data with the antennas directly coupled against the ice; while line 02 contains data attained with antennas suspended approximately 50cm above the lake surface.

Survey properties

Key properties of the GPR survey are displayed in Table 1 and were determined to produce the best subsurface image possible. Access to 200MHz antennas was the highest frequency available for the PulseEKKO PRO system and was chosen because it would provide the best resolution. While higher frequencies tend to attenuate more rapidly than lower frequencies (Annan, 1996); depth of penetration was not a concern for this survey due to the low loss nature of a frozen, fresh water environment. The remainder of the properties were chosen based on the recommended setup for a 200 MHz system as instructed in the Sensoft instruction manual (Sensors and Software, 2001) for ideal performance.

INTERPRETATION

Raw GPR data attained for this survey is shown in Figure 9 and Figure 10 for lines 1 and 2 respectively. These images show diffractions caused by the reflectors frozen into the base of ice, and reflections caused by the lake bottom and the approximate location of the ice-water interface. Processing these lines is expected to increase the quality of the received signal and enhance the ability to correlate the two sets of data.

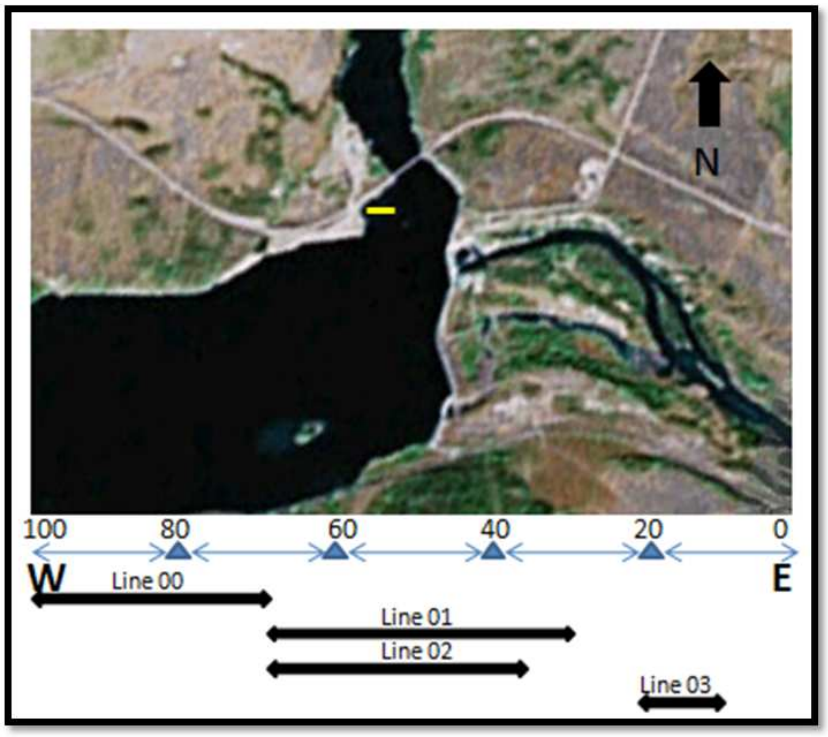

FIG. 8. Location of survey lines shown in yellow. Triangles represent submerged and frozen rocks relative to survey lines.

Time window	300 ns
Step Size	0.1 m
Nominal Frequency	200 MHz
Antenna Separation	1 m
Number of Stacks per trace	64
Sample rate	0.4 ns

Table 1. Survey properties.

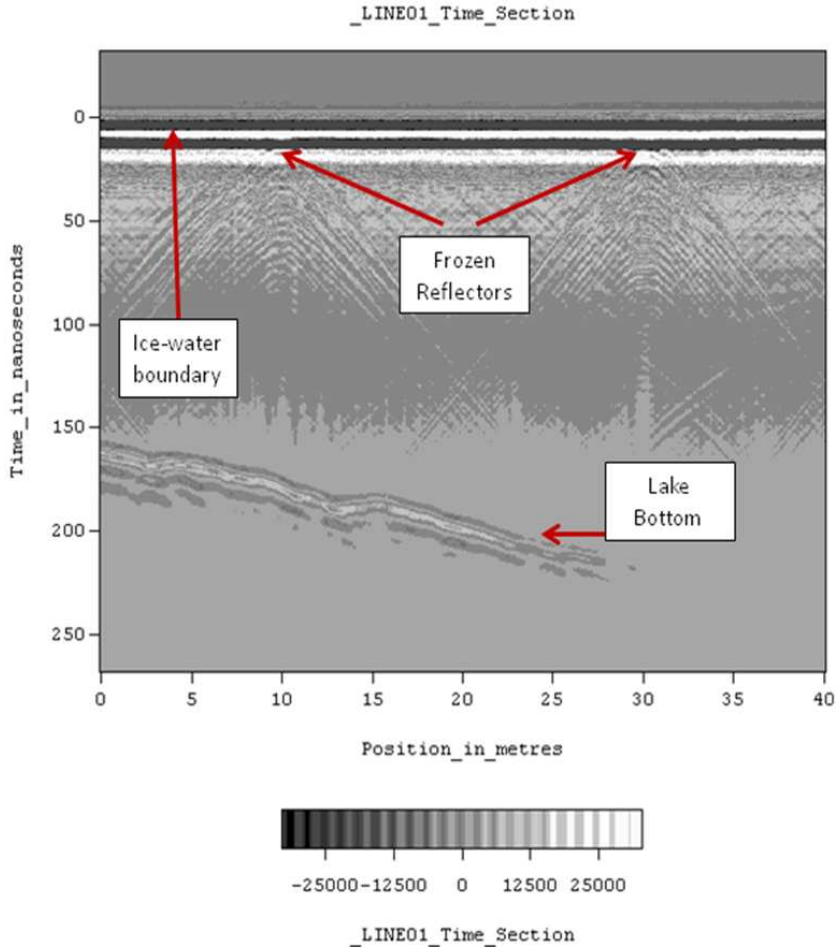

FIG. 9. Raw GPR data from line 01. Antennas coupled with the ice.

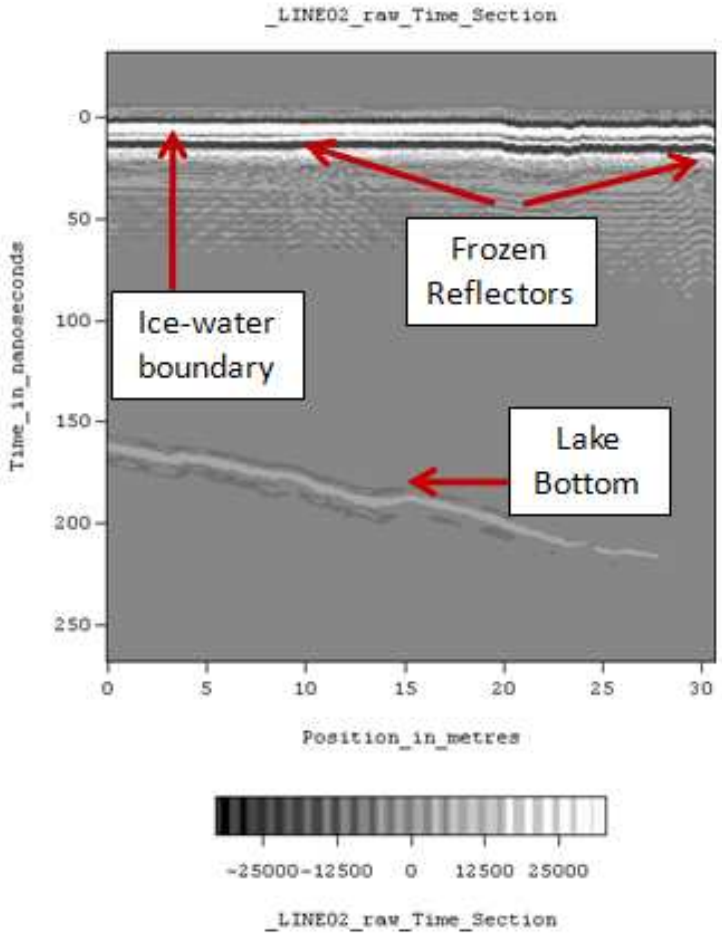

FIG. 10. Raw GPR data from line 02. Antennas coupled with the ice.

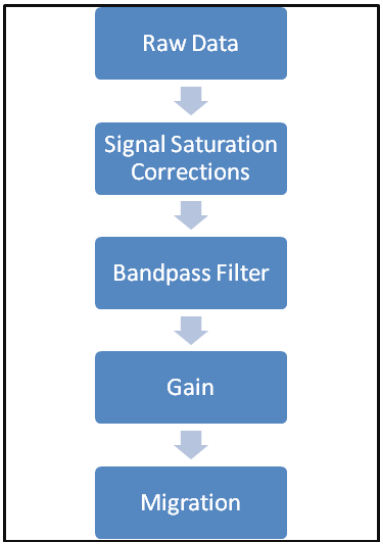

FIG. 11. Processing workflow.

DATA PROCESSING

The workflow for processing GPR data is shown in Figure 11 and was determined based on the papers Fisher et al. (1992) and Sensors and Software (2001).

Signal Saturation Correction

Inductive coupling between the transmitting and receiving antennas becomes problematic when the antenna spacing is small (Allred et al., 2008). Large amounts of energy are received from direct arrivals, and near surface reflections which induces a low frequency component to each trace (Fisher et al., 1992). The higher frequency reflections are superimposed on this exponential decay which makes the important events less distinguished (Fisher et al., 1992). "This low frequency component is removed by running an average filter on each trace. Within a window width, the average value of all data points is determined and removed from the centre point. As this window moves throughout the trace this artifact is removed (Sensors and Software, 2001)." Figure 12 shows an original raw trace, and Figure 13 displays the same trace after the signal saturation correction has been applied.

Bandpass filtering

Bandpass filtering is a common practice in GPR data processing because it lets through data in a specified frequency range while removing out of band noise (Fisher et al., 1992). Cut off frequencies were determined by analyzing amplitude spectra (Figure 14, Figure 15) and the underlying assumption that "GPR systems are designed to achieve bandwidths that are about equal to the centre frequency" (Davis and Annan, 1989). Note that the amplitude spectrum of line 2 has a distinctive feature at 120 MHz. This notch in the amplitude spectrum is unique to data acquired with elevated antennas and will be discussed later. The frequency band that produced the best result was 20/30-220/230.

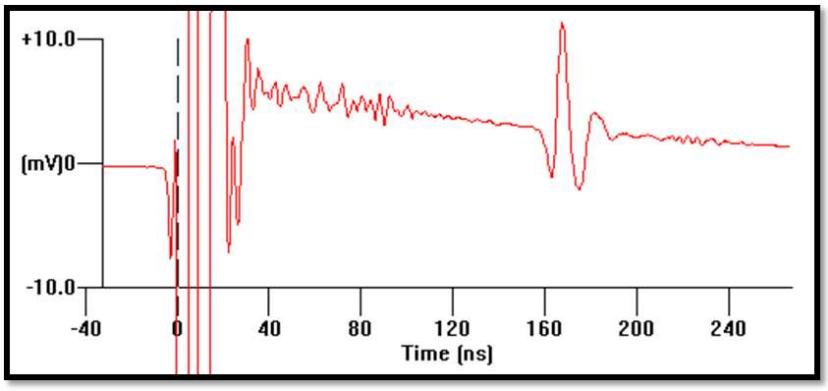

FIG. 12. Line01, Trace 30-Raw.

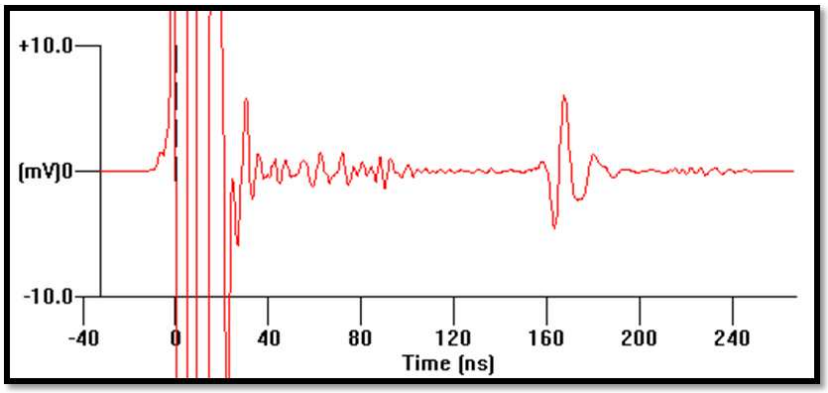

FIG. 13. Line01, Trace 30-After signal saturation correction.

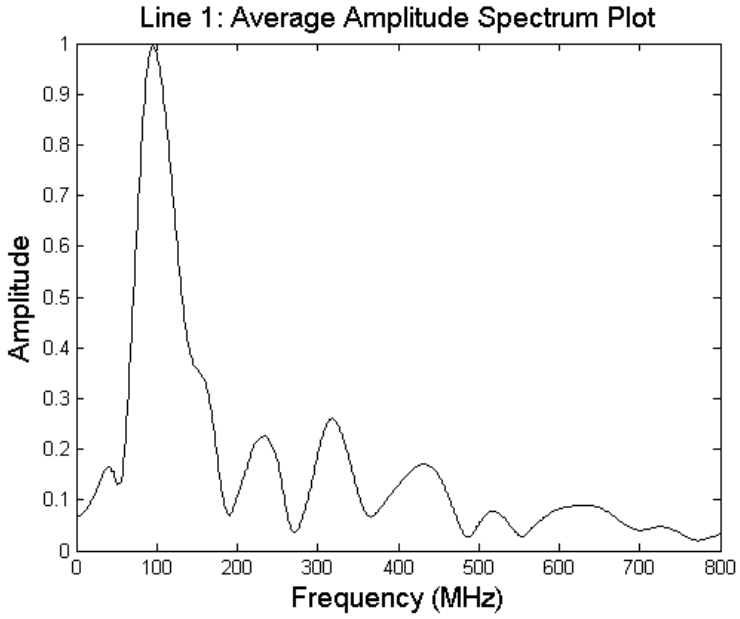

FIG. 14. Amplitude spectrum of line 1.

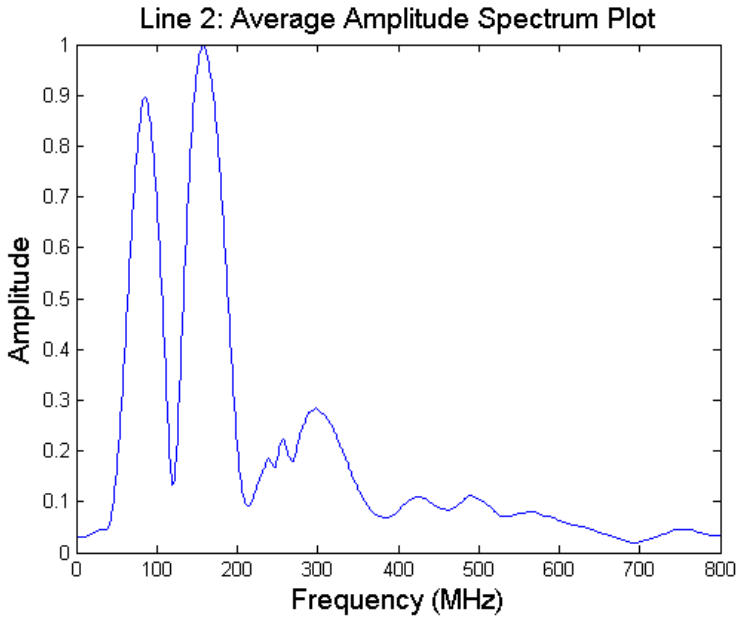

FIG. 15. Amplitude spectrum of line 2. Note the notch in the data at 120 MHz

Figure 16 and Figure 17 shows the result of bandpass filtering which produced a notable improvement in the image. This is most clearly seen in line 2 within the 40-80ns time range where a banding effect was removed (Figure 18).

Gain

Gain functions were used to improve the display of GPR sections by accounting for attenuation and geometric spreading (Allred et al., 2008). An automatic gain control (AGC) function with a maximum gain of 50 dB was found to produce the best result. Signals from known reflectors were enhanced while noise was kept to a minimum.

Migration

"The migration process applies a synthetic aperture reconstruction process to the data set (Sensors and Software, 2001)". This processing technique is supposed to collapse scattered signals such as hyperbolic diffractions to isolated points which can improve the spatial accuracy of the data set (Lee, 2003). Poor to marginal results were obtained from migration which stemmed from banding in the data and software limitations. Win Ekko Pro software only allowed the user to input single velocity for the model, and a spatial offset value (which is strongly recommended by the manufacturer to be left at default) into the migration algorithm. The assumption of a constant velocity model to migrate the data for this dataset is highly inaccurate due to the extreme velocity contrast between ice and water.

Using trial and error, numerous values were used in the migration algorithm. The best image was produced using the velocity of water (0.03m/ns) (Figure 19 and Figure 20). These images are a marginal improvement over unmigrated data and were evaluated based

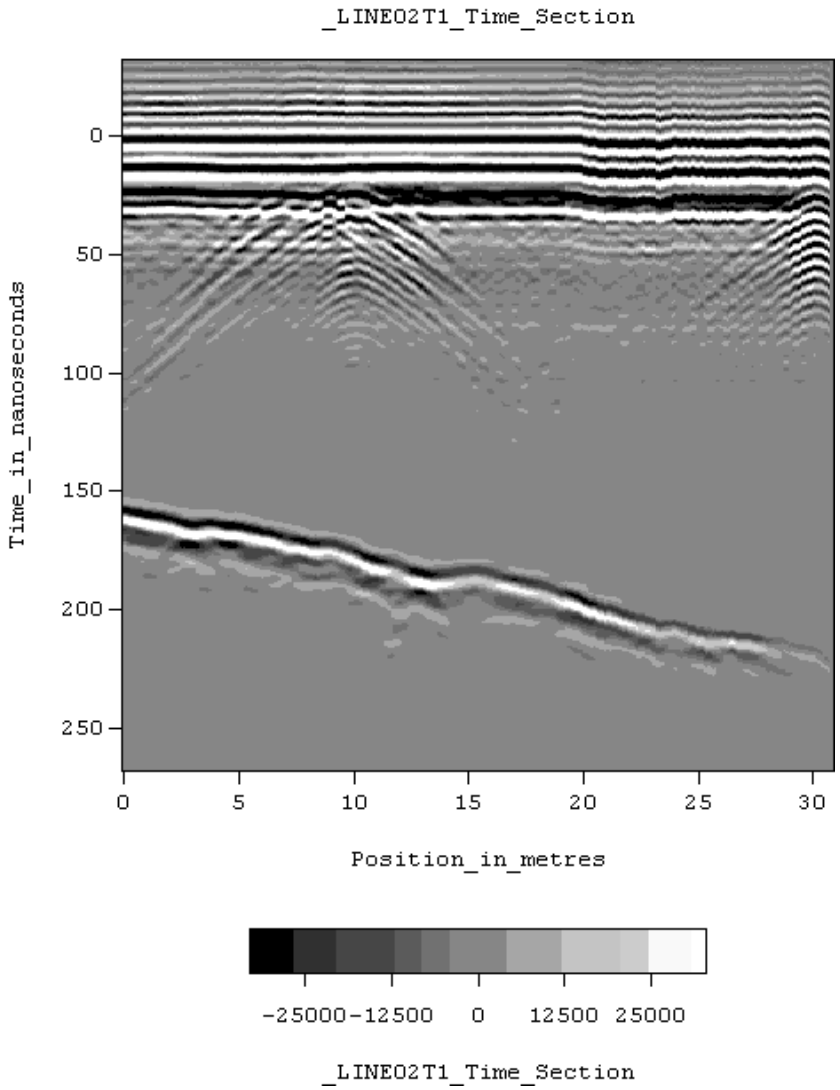

FIG. 16. Line01 with saturation correction, bandpass filter, and an AGC applied to the raw data.

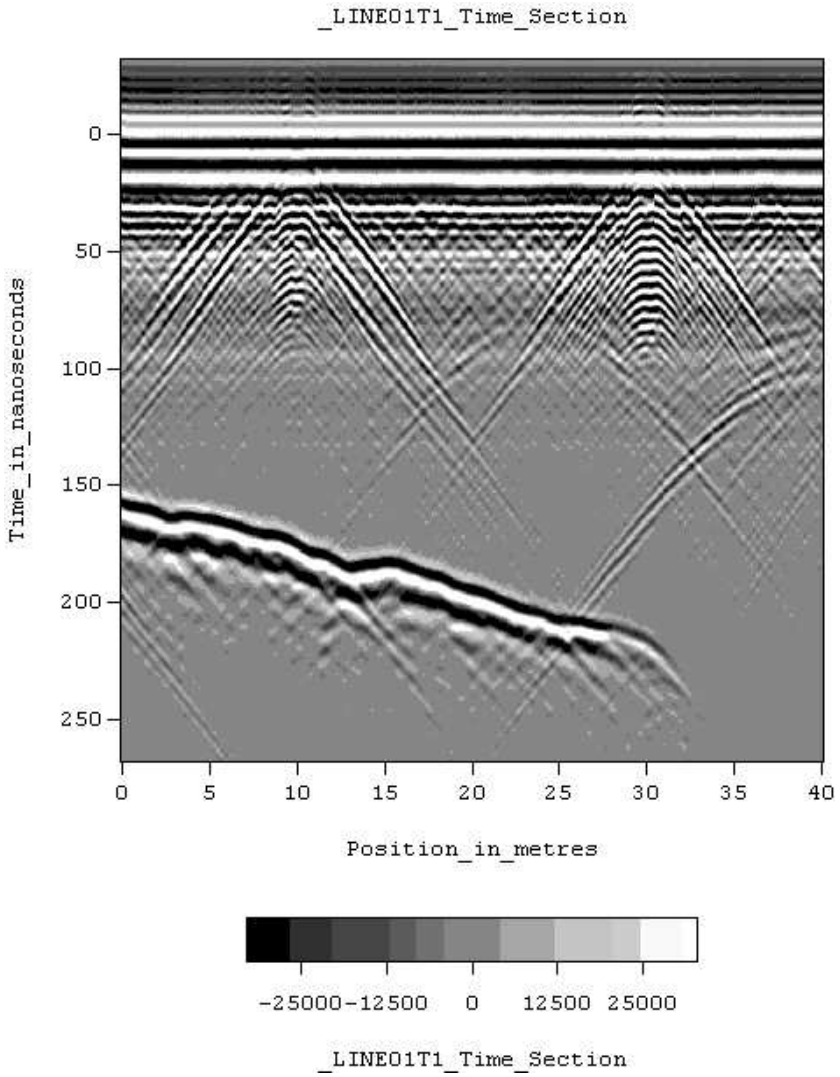

FIG. 17. Line02 with saturation correction, bandpass filter, and AGC applied to raw data.

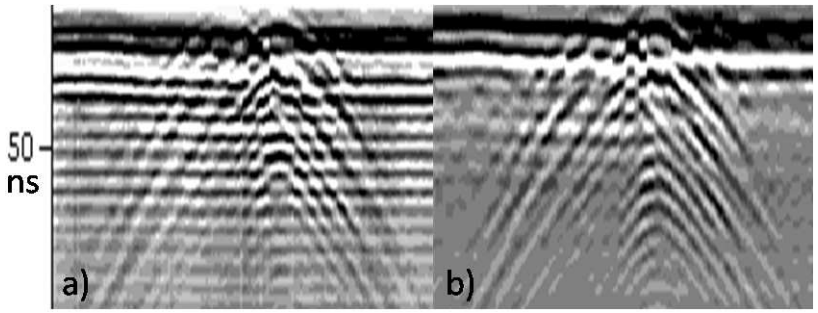

FIG. 18. Line 02 a) Without a bandpass filter. b) With a bandpass filter.

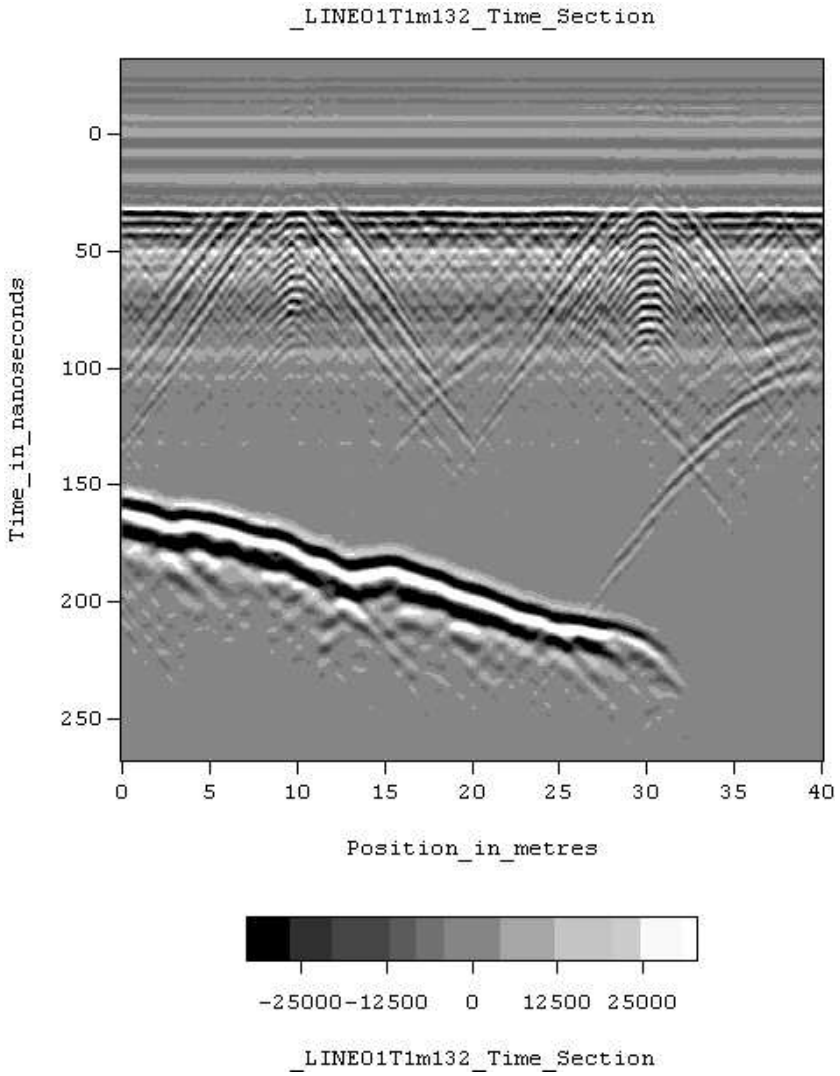

FIG. 19. Line 01 migrated.

on its inability to collapse the diffractions cause by the submerged rocks. Diffractions caused by the lake bottom were the only event that was noticeably collapsed. It was expected that the best velocity to be used for migration would be v_{ice} since the rock is positioned at the bottom of the ice layer. However the resultant migration was extremely noisy and the hyperbolas from the rocks were still not collapsed.

ICE COUPLED VS. SUSPENDED COMPARISON

Analysis of Submerged Rock Diffractions

An initial objective of this project was to use migration to collapse the hyperbolic diffractions caused by the submerged rocks to points (Figure 21). With the travel times obtained from these points in migrated data, one could use known ice thickness to determine the velocity of ice or vice versa, literature values for velocity could be used to determine ice thickness. Such values could be compared to literature and measured values

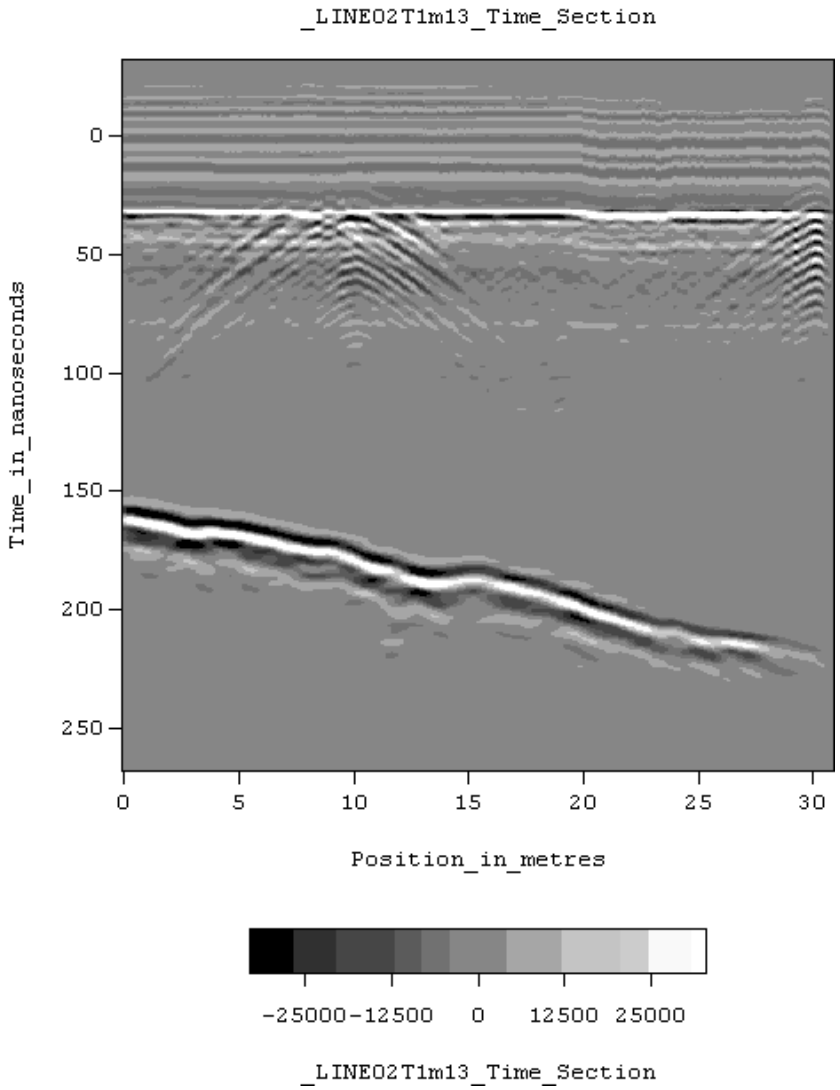

FIG. 20. Line 02 migrated.

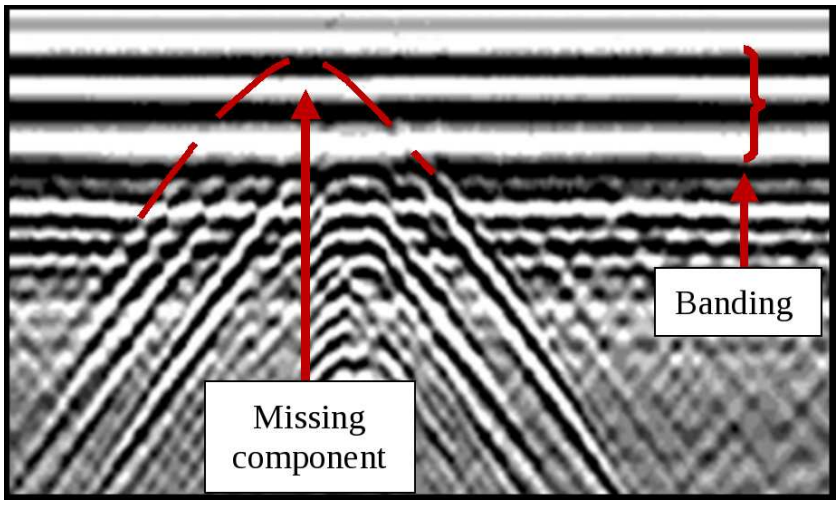

FIG. 21. Close up of hyperbolic diffraction cut off by ringing of direct arrivals.

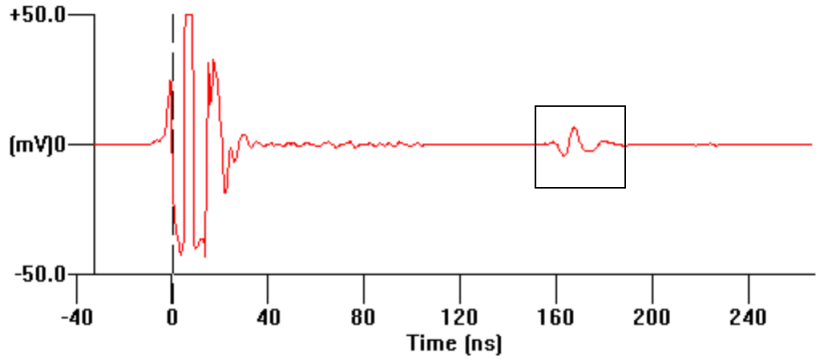

FIG. 22. Line 01 trace at 2.7m. The reflection caused by the lake bottom is boxed

respectively, and provide a qualitative assessment of the two acquisition methods. However, high amplitude ringing caused by the direct arrivals has wiped out the apex of the hyperbolic signal associated with reflections from the rocks (Kim et al., 2007). Without knowing the precise location of this apex, it is not possible to attain an accurate travel time and interpret these diffractions.

Relative Trace amplitudes

A qualitative test of the modelled results in Figure 3 is a comparison of traces shot at the same location using the two antenna coupling systems. Figures 22 and 23 represent traces shot at 2.7m along the lines using ice-coupled and suspended antennas respectively. Due to the inability of the Pulse EkkoPRO to resolve the ice-water contact caused by massive ringing of the direct arrivals, only the reflection off the lake bottom will be analyzed. The impulse response model (Figure 3) speculated a slight decrease in reflected amplitude for the suspended case at the lake bottom. Comparisons of traces in both GPR lines consistently show this result (Figures 22 and 23).

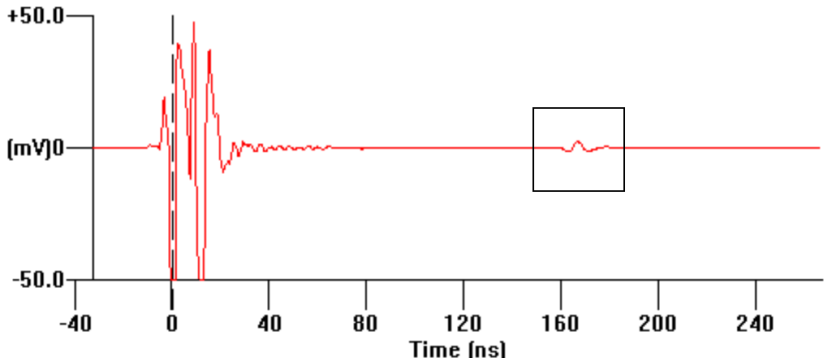

FIG. 23. Line 02 trace at 2.7m. The reflection caused by the lake bottom is boxed.

Amplitude spectra

The most notable difference between the two datasets acquired for this experiment is the resultant amplitude spectrum. Spectra for GPR surveys are expected to have a signal band similar to that shown in Figure 14. The notched spectrum of the elevated data (Figure 15) suggests that there is a type of destructive interference occurring for signals with a 120 MHz frequency when the antennas are elevated. This notch has a negative effect on the data because this frequency should have a high amplitude value. It is approximately half of the 200 MHz frequency transmitted by the antennas, and is thus within the expected frequency band (Davis and Annan, 1989).

Sensitivity to Noise

Elevating the GPR antennas also appears to increase susceptibility to detecting noise. This is hypothesized from information obtained when the band pass filter was applied to both datasets, and only a significant improvement in the elevated antenna data (line 2) was observed. Band pass filters are designed to remove out of band noise that is lower and higher than the expected signal band (Margrave, 2010).

It is believed that the 16bit dynamic range of the system will be more prone to detecting noise when the antennas are elevated. Dynamic range is the ratio between the smallest and largest amplitude that the device can detect, and needs to be considered in all GPR datasets (Daniels, 2004). Elevating the antennas has been modelled to reduce the amplitude of the ice-water reflection significantly more than the reflections caused by other boundaries. Since this boundary causes the largest amplitude reflection, the systems dynamic range should be more capable of detecting lower amplitude noise.

A potential problem with this hypothesis is that the amplitudes of direct arrivals will not differ between the two acquisition methods due to constant antenna separation. These arrivals are the absolute maximum amplitude events that the receiver detects. The pulsEKKO pro systematically clips these direct arrivals which increase the system's ability to sense lower amplitudes. This happens since the largest amplitudes recorded has been reduced, and thus the systems fixed dynamic range will be able to detect more subtle events (Jol, 2009). Due to the unknown process of the clipping operation performed by the PulseEKKO

Pro, this hypothesis cannot be tested. Depending on the algorithm used, the direct arrivals may be differentially clipped depending later signals. This would not allow an accurate comparison between datasets. Shielding the antennas would be a great way to test this and improve data quality. Shielded antennas reduced the impact of direct arrivals and limit noise from external sources (Daniels, 2004).

Ringing

Ringing is the periodic arrival of a strong signal which is caused by resonance of the antennas (Allred et al., 2008). Such an artifact in the data can cause deeper signals to become irresolvable. The submerged point reflectors along the survey line experienced sever ringing which resulted from light waves inability to penetrate a metal foil which was covering the rocks (Sato, 2001). In the future, metal objects should be avoided as reference points along a GPR survey to ensure that deeper structures are not lost due to ringing.

CONCLUSIONS

Several differences and similarities in data quality were observed when two near surface GPR acquisition methods were used. Methods involved directly coupling the antennas with the ice, and elevating the antennas 0.5 m above the ground. The overall result of elevating the antennas from the ground was a degradation of the raw data. Processing was shown to be more effective on elevated datasets and the resultant image became more comparable to the ice-coupled dataset.

A significant difference between the two datasets was observed in the amplitude spectra. A notch in the spectra occurred in the elevated antenna dataset (line 2) at 120 MHz. This indicates that the signal encountered destructive interference at this frequency, which reduced its signal strength. 120 MHz lies within the expected signal band and should contain high amplitude information (Davis and Annan, 1989). In the ice-coupled dataset, this low amplitude feature is not present in the spectra.

Both acquisition methods produced similar images after processing from an interpretation standpoint. Elevated and ice-coupled datasets experienced significant banding which eliminated the ability to interpret the important ice-water interface and the submerged point reflectors. This was the largest problem in the experiment and the antenna position of the GPR system did not affect the result. Future works in frozen environments need to eliminate direct arrival ringing to resolve shallow events.

MATLAB MODELLING CODE

```
% Impulse Response modeller for a 4 layered case
%n=sqrt(dielectric constant)=index of refraction

n1=1;%Air
z1=0.5; %Elevation of the antennas
n2=2; %Ice
z2=0.55; %Ice Thickness
```

```
n3=9; %water
z3=7;% Water layer thickness
n4=5; %Lake floor

p=0:0.02:0.9 %Representative ray parameters

theta1=asind(p./n1) %take off angle 0-45 degrees/incidence angle at air-ice interface
theta2=asind(p./n2) %incidence angle at ice-water interface
theta3=asind(p./n3)%incidence angle at water-lake bottom interface
theta4=asind(p./n4); %transmission angle at lake bottom

Z1=n1*cosd(theta1); %radar impedance for layer 1
Z2=n2*cosd(theta2); %radar impedance for layer 2
Z3=n3*cosd(theta3); %radar impedance for layer 3
Z4=n4*cosd(theta4); %radar impedance for layer 4

%SITUATION #1 (ELEVATED ANETENNAS)
%Air-Ice-Water-Ground Case
x1=2*(tand(theta1)*z1+tand(theta2)*z2+tand(theta3)*z3);
%antenna spacing for various ray paths

R1=(Z1-Z2)./(Z1+Z2); %reflection coefficient calculation
T1=2*Z1./(Z1+Z2); % transmission coefficient calculation
R2=(Z2-Z3)./(Z2+Z3); %reflection coefficient calculation
T2=2*Z2./(Z2+Z3); % transmission coefficient calculation
R3=(Z3-Z4)./(Z3+Z4); %reflection coefficient calculation
R_net_soil=(1-R1).*(1-R2).*-R3.*(1+R2).*(1+R1); %Impulse response
hold on
plot(x1,R_net_soil,':k')
title('Modelled Impulse Response at Interfaces (Without Attenuation)')
xlabel('Antenna Offset (m)')
ylabel('Impulse Response')
axis([0 1.5 -0.4 1])

%Air-Ice-Water Case
x2=2*(tand(theta1)*z1+tand(theta2)*z2); %antenna spacing
R1=(Z1-Z2)./(Z1+Z2); %reflection coefficient calculation
T1=2*Z1./(Z1+Z2); % transmission coefficient calculation
R2=(Z2-Z3)./(Z2+Z3); %reflection coefficient calculation
R_net_water=(1-R1).*-R2.*(1+R1); %impulse response
plot(x2,R_net_water,':g')

%Air-Ice Case
x3=2*(tand(theta1)*z1); %antenna spacing
R1=(Z1-Z2)./(Z1+Z2); %reflection coefficient calculation
R_net_ice=-R1; %Impulse Response
```

```
plot(x3,R_net_ice,':b')
legend('Soil','Water','Ice')

%SITUATION #2 (ICE COUPLED)
p2=0:0.05:1.9; %New Ray parameters
theta2=asind(p2./n2) %take off angle 0-44degrees
theta3=asind(p2./n3);
theta4=asind(p2./n4);
Z2=n2*cosd(theta2); %radar impedance for ice
Z3=n3*cosd(theta3); %radar impedance for water
Z4=n4*cosd(theta4); %radar impedance for lake bottom

%Ice-Water-Ground Case
x2=2*(tand(theta2)*z2+tand(theta3)*z3); %antenna spacing

R2=(Z2-Z3)./(Z2+Z3); %reflection coefficient calculation
R3=(Z3-Z4)./(Z3+Z4); %reflection coefficient calculation
R_net_soil=(1-R2).*-R3.*(1+R2);
plot(x2,R_net_soil,'k')

%Ice-Water Case
x3=2*(tand(theta2)*z2); %antenna spacing
R2=(Z2-Z3)./(Z2+Z3); %reflection coefficient calculation
R_net_water=-R2;
plot(x3,R_net_water,'g')

legend('Soil (Elevated)','Water (Elevated)','Ice (Elevated)', 'Soil (Coupled)','Water
hold off
```

REFERENCES

Allred, B. J., J. J. Daniels, and M. R. Ehsani, 2008, Handbook of agricultural geophysics: CRC Press.

Annan, A. P., 1996, Transmission dispersion and gpr: JEEG, **0**, 125–136.

Barger, V. and M. Olsen, 1987, Classical electricity and magnetism: Allyn and Bacon Inc.

Carter, S. P., D. D. Blankenshipb, D. A. Young, M. E. Peters, J. W. Holt, and M. J. Siegert, 2009, Dynamic distributed drainage implied by the flow evolution of the 1996-1998 adventure trench subglacial lake discharge: Earth and Planetary Science Letters, **283**, 24–37.

Daniels, D. J., 2004, Ground penetrating radar 2nd edition: Institute of Electrical Engineers.

Davis, J. L. and A. P. Annan, 1989, Ground penetrating radar for high resolution mapping of soil and rock stratigraphy: Geophysical Prospecting, **37**, 531–551.

Finlay, P. I., N. S. Parry, S. A. Proskin, and R. J. Mickle, 2008, An overview of ice profiling using ground penetrating radar (gpr): SAGEEP Proceedings, 461–470.

Fisher, S. C., R. R. Stewart, and H. M. Jol, 1992, Processing ground penetrating radar (gpr) data: Crews Research Report, **4**, 1–22.

Grasmueck, M., R. Weger, and H. Horstmeyer, 2005, Full-resolution 3d gpr imaging: Geophysics, **70**, K12–K19.

Jol, H. M., 2009, Ground penetrating radar: Elsevier.

Kim, J. H., S. J. Cho, and M. J. Yi, 2007, Removal of ringing noise in gpr data by signal processing: Geophysics Journal International, **11**, 75–81.

Lee, H., 2003, Overview of synthetic aperature image reconstruction algorithms for gpr imaging with pulse-echo and step frequency fmcw systems: JEEG, **8**, 105–113.

Margrave, G. F., 2010, Methods of seismic data processing: CREWES.

Mitchell, P., 1991, Atlas of alberta lakes 1st edition: University of Alberta Press.

Saarenketo, T. and T. Scullion, 2000, Road evaluation with ground penetrating radar: Journal of Applied Geophysics, **43**, 119–138.

Sato, M., 2001, Gpr and its application to environmental study. http://cobalt.cneas.tohoku.ac.jp/users/sato/.

Sen, M. K., P. L. Stoffa, and R. K. Seifoullaev, 2003, Numerical and field investigations of gpr: Towards an airborne gpr: Subsurface Sensing Technologies and Applications, **1**, 41–60.

Sensors and Software, 2001, Win_ekko user guide v1.0.

Waite, A. H. and S. J. Schmidt, 1961, Gross errors in height indication from pulsed radar altimeters operating over thick ice or snow: IRE, 1515–1520.